

Article

# Lube Oil Wear Reduction via Organic Tribofilms

Nurul Athirah Ismail and Samira Bagheri \* 

Nanotechnology & Catalysis Research Centre (NANOCAT), IPS Building, University of Malaya, 50603 Kuala Lumpur, Malaysia; tira.athirahismail@gmail.com

\* Correspondence: samira\_bagheri@um.edu.my; Tel.: +60-176-153-692

Received: 20 July 2017; Accepted: 4 August 2017; Published: 9 August 2017

**Abstract:** Effective tribofilms are desirable to protect mechanical systems. In the research, the reduction in wear and friction were investigated through the use of organic additives. Graphene-based organic additives were prepared by surface modification of graphene using organic moiety that will provide tribochemical reaction with rubbing metal surface. The role of surface protective additives becomes vital when operating conditions become severe and moving components operate in a boundary lubrication regime. After protecting film is slowly removed by rubbing, it can regenerate through the tribochemical reaction of the additives at the contact. Many researchers demonstrated that organic additives physically or chemically adsorbed on rubbing metal surfaces to form monolayers, with their shear strength deriving primarily from the weak van der Waal interactions between opposing hydrocarbon chains at the interfaces. Experiments were conducted on a base oil where 0.01 wt % of the additive was used. Tribological evaluation was conducted using four-ball tester under room temperature and the morphology of the worn surfaces were characterized using Field emission scanning electron microscopy (FESEM). Experimental results showed a 16% reduction in friction and 30% reduction in wear when compared to the base oil containing no additive.

**Keywords:** organic; tribofilms; additive; lube oil; wear; tribochemical

## 1. Introduction

Fuel economy is one of the major factors that speeds up research in the formulation of lubricant and lubricant additives. To put it simply, the reduction in fuel consumption is named fuel economy. An increase in combustion efficiency and friction reduction in the transmission and engine can lead to fuel economy [1]. An increase in transportation activities has consumed significant portions of our energy resources. And most of the energy produced is used to overcome friction in moving mechanical systems [2]. Friction can result in both advantageous and disadvantageous ways. When driving and braking cars on the road, we depend on friction. However, in the context of lubrication and tribology, friction and wear is an unwanted phenomenon that occurs when close contact of surfaces occurs in relative motion [3]. Friction and wear are the two major causes for energy and material losses in mechanical processes [4]. To improve the effective functioning of mechanical components or two surfaces in contact, better lubricant along with chemical additives is required. In military combat operations, extreme tribological environment is required [5]. For the protection of mechanical components, from friction and wear in aerospace, automotive, military and various industrial applications, an efficient lubricant is demanded. Moreover, the technology of protecting machines entirely depends on the quality of lubricants. The addition of nanomaterials as additives in base lubricant oil is a rapidly progressing field of research, because nanomaterials are different from traditional bulk materials due to their extremely small size and high specific surface area [6]. Different researchers have tried a variety of nanomaterials dispersed base oils to improve the wear and friction reduction [7,8].

Low wear and friction can be generated by the material with low shear strength,  $S$  and high surface hardness,  $H$ . To have a low shear strength, the layers of the materials must be very thin. Therefore, low friction can be achieved if thin layers of materials with hard surfaces and low shear strength are used [9]. The layers of the material must be very thin, in order not to increase the contact area,  $A_c$  [10]. Materials that can fulfil these requirements are commonly found in inorganic compounds. Therefore, in this study, graphene or graphene oxide is used as the base material in preparing the solid organic tribofilms for reduction of friction and also wear. An ideal sheet of graphene consists of a 2D honeycomb structure of carbon atoms in a single layer [11]. It was confirmed that graphene has extremely high rigidity and breaking strength. The values calculated corresponds to Young's modulus of  $E = 1.0$  TPa and intrinsic strength of 130 GPa, proving that graphene is one of the strongest material ever determined [12]. Graphene has been tested and proved to be one of the strongest materials ever measured [13]. Graphene being two-dimensional material, offers unique friction and wear properties that is not typically seen in conventional materials. Its high chemical inertness, extreme strength and easy shear capability on its densely packed and atomically smooth surface are the major favourable attributes for its impressive tribological behaviour. Because of its high load-bearing limit, high chemical steadiness, low surface energy, strong intramolecular and weak intermolecular bonding, nanocarbon materials have gained incredible attention by tribology scientists. Graphene had also been the focus of enthusiasm in studies because of its excellent properties and unique structure.

Only a few reviews on graphene in tribology and mechanical applications have been reported so far [14]. Also, a few scientists have revealed that graphite [15] and some of the graphite derivatives [16] together have the desirable properties mentioned earlier. The tribological properties of graphite nanosheets as an oil additive has been explored by Lin et al. [17]. In between layers of graphite, there is weak interatomic interaction, van der Waals forces and low shear stress [18]. The properties of graphite as an additive for lube oil has been investigated and found that to have some improvement in the reduction of friction and wear when graphite or graphite derivatives were introduced into the oil at optimum concentration [19]. Philip et al. have studied effect of graphite and carbon nanofibers as additives on the performance efficiency of gear pump driven hydraulic circuit using ethanol solution. They claim that both graphite and carbon nanofibers dispersions in ethanol within a concentration range of 195–1500 ppm can maintain hydraulic circuits with increase pump efficiency without modifying the viscosity of the ethanol [20]. Zhang et al. has reported 17% and 14% reduction in frictional coefficient and wear, respectively, with oleic acid-modified graphene as lubricant additive [21]. Ou et al. studied tribological properties of reduced graphene oxide (RGO) sheets on silicon substrate synthesized via covalent assembly [22]. They attributed the wear and friction reduction of RGO to its self-lubricating property. Similarly, Lee et al. have demonstrated the generality of the tribological results on thinnest graphene sheets, which indicates that this may be a universal characteristic of nanoscale friction for atomically thin materials weakly bound to substrates using frictional force microscopy [13].

From an application point of view, nanolubricants are technologically important because of their usage in various industries. Even though reports were already present on nanolubricants, they suffer from low efficiency. Hence, it is always essential to improve the efficiency of lubricants. Studies show that the graphene platelets are a failure as oil additive at higher temperatures, and this could be due to the damaging of the protective film formed by the graphene at higher temperatures, and also due to a significant increase in agglomerations within the lubricant [17]. Therefore, the application thus far is considerable restricted. Nevertheless, the issue with dispersion stability can be resolved by utilising some chemical and physical methods. The solution to this would be the addition of a dispersant or modification that will reduce the agglomeration and improve the dispersive ability in the lubricant [14]. Therefore, in this study, organic moiety was introduced on the surface of GO which act as the base for solid inorganic additive in order to provide the organic tribofilms and at the same time improve their dispersion in base oil.

## 2. Experimental Methods

### 2.1. Materials

Graphene oxide, 1-bromodecane, 1-bromooctane, 1-bromododecane and sodium azide ( $\text{NaN}_3$ ) were purchased from Sigma-Aldrich (Germany). Tetrahydrofuran (THF), dichloromethane (DCM), diethyl ether, dimethyl formamide (DMF), dimethyl sulphoxide (DMSO), and trimethylamine ( $\text{Et}_3\text{N}$ ) were purchased from Friedemann Schmidt. Sodium hydride ( $\text{NaH}$ ), dimethyl malonate, lithium aluminium hydride ( $\text{LiAlH}_4$ ), magnesium sulphate ( $\text{MgSO}_4$ ), chloroform and thionyl chloride ( $\text{SOCl}_2$ ) were purchased from Merck. Dichloromethane (DCM), sodium ascorbate and copper sulphate pentahydrate ( $\text{CuSO}_4 \cdot 5\text{H}_2\text{O}$ ) were purchased from Fischer Scientific and propargyl bromide was purchased from Sigma Aldrich.

### 2.2. Materials Preparation

Three major steps were involved in preparation of materials as shown in Figure 1. For the first step, alkyne-functionalized GO,  $\text{GO}_f$  was synthesized. Firstly, DiPPOH (dimethyl malonate and propargyl bromide) was prepared by using dimethyl malonate and propargyl bromide as the starting materials. In an ice bath, dimethyl malonate was added to a sodium hydride suspension (60 wt % in mineral oil) in dry THF followed by propargyl bromide (80 wt % in toluene). The mixture was left stirred overnight and then extracted using water and followed by dichloromethane. The combined organic phase was concentrated using a rotary evaporator, leaving dimethyl 2,2-di(propynyl)malonate, DiMDiPM as the product. The DiMDiPM was then stirred in anhydrous THF.  $\text{LiAlH}_4$  was added to the stirred solution and the mixture left stirred for overnight. Water and 10%  $\text{NaOH}$  solution was added carefully to stop the reaction [23]. The mixture was filtered and the filtrate was dried using  $\text{MgSO}_4$ . Concentrate the product using a rotary evaporator to have the 2,2-dipropargyl-1,3-propanediol, DiPPOH.

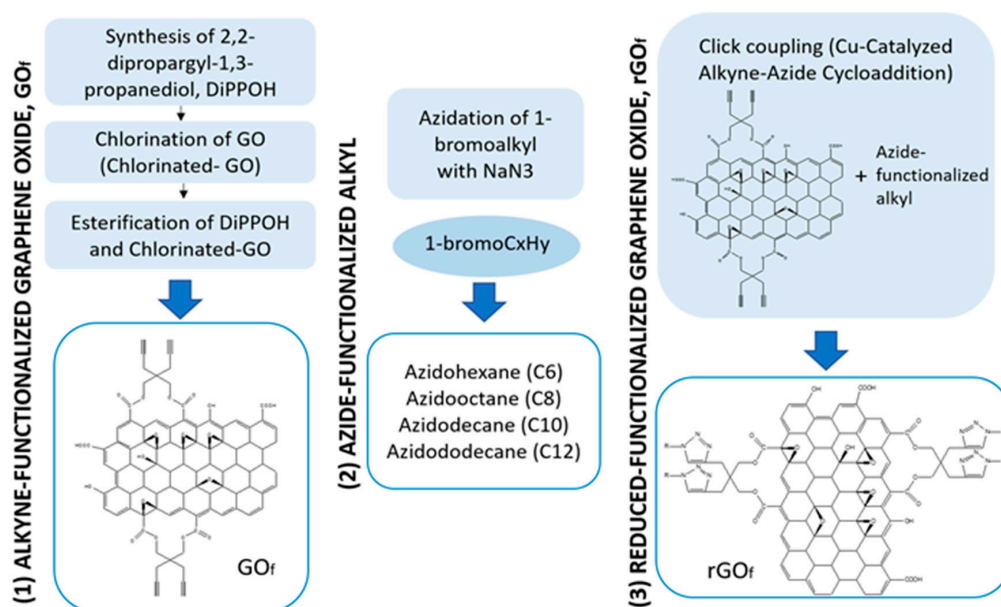


Figure 1. The overview on materials preparation.

Graphene oxide was stirred in chloroform. In an ice bath thionyl chloride and trimethylamine was added dropwise into the mixture [24,25]. The mixture was then stirred for 2 h and further concentrated using a rotary evaporator to produce chlorinated GO. In anhydrous THF,  $\text{NaH}$  was added followed by the chlorinated GO and DiPPOH prepared. The mixture was stirred overnight then concentrated using a rotary evaporator to produce alkyne-functionalized graphene oxide,  $\text{GO}_f$ .

The second step required is to prepare azide-functionalized alkyl. 1-bromohexane and anhydrous sodium azide added into DMF and the reaction mixture was stirred at 80 °C under reflux for overnight [26]. The mixture was then extracted using water and diethyl ether. The combined organic phases were added with  $\text{MgSO}_4$  to remove water. The mixture was filtered and the filtrate was concentrated by rotary evaporator to give 1-azidohexane as the product. The 1-bromohexane was replaced by 1-bromooctane, 1-bromodecane and 1-bromododecane with same procedure to give the product of 1-azidooctane, 1-azidodecane, and 1-azidododecane respectively.

The final step in the preparation of materials is the cycloaddition reaction between the azide and alkyne group. The prepared alkyne-functionalized graphene oxide and four different azide-functionalized alkyls followed by sodium ascorbate were added to the mixture of water and DMSO (20:10) and sonicated for 1 h.  $\text{CuSO}_4 \cdot 5\text{H}_2\text{O}$  was added and then sonicated for 2 h. The mixture was stirred overnight and then wash with water and ethanol [27–29]. The product dried overnight and give reduced-functionalized graphene oxide,  $\text{rGO}_f$  as the final product.

### 2.3. Materials Characterization

Fourier-Transform Infrared (FTIR) spectra are obtained using a Perkin-Elmer FTIR spectrophotometer within the wave number in the range of 4000–400  $\text{cm}^{-1}$ . Samples are finely ground with potassium bromide, KBr and then compressed into pellet form. PANalytical diffractometer used to obtain the pattern of X-ray diffraction (XRD) of the sample with a  $2\theta$  angle ranging from 5 to 50° and scan rate of 10°/min. Thermal Gravimetric Analysis (TGA) with thermal analyzer under an inert atmosphere in the range of 50 to 800 °C was performed at a heating rate of 10 °C/min.

### 2.4. Tribological Characterization

Group II 500 N petroleum-based oil was used in the preparation of lubricant oil. The prepared additives material were added in the base oil at 0.01 wt %, and transferred into a blending flask. The flask was immersed in the Thermo-6D ultrasonic bath. An RW20IKA mechanical stirrer (IKA, Wilmington, NC, USA) was used with 2 blade propellers, and was inserted into the mixture flask. The mixture was stirred at a rate of 300 rpm at 60 °C under 40 kHz ultrasonic frequency for an hour to confirm the complete mixing and dispersion of both components.

The four-ball tester were used to determine the tribological behavior of the synthesised materials. The main measurement of four-ball tester was to determine the wear preventive properties, extreme pressure properties and the friction behaviour of lubricant oil. This experiment used the Ducom Four-ball Instrument, while the balls were AISI 52-100 steel balls (USA) with a diameter of 12.7 mm and 64–66 Rc hardness. ASTM D2783 standard method was followed for the tribological characterizations using the aforementioned four-ball instrument. The test conditions for this standard include room temperature at a speed of 1200 rpm, load 400 N and test duration of 60 min.

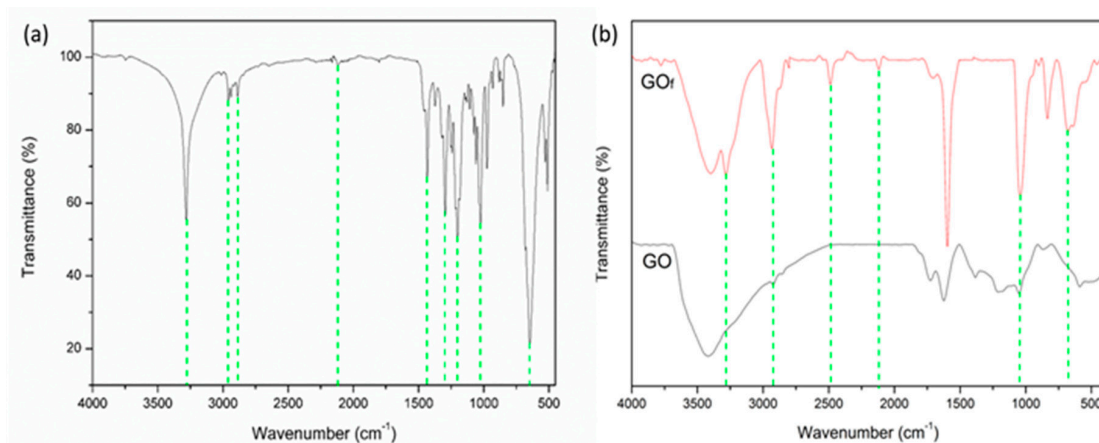
At the end of four-ball test, the ball bearings were collected and washed with acetone, then dried in an oven for an hour at 70 °C. The wear scar on the three stationary ball bearings surface were analysed using scanning electron microscopy (SEM) spectroscopy. The metallograph were analysed and expressed as wear scar diameter (WSD). The SEM images of the wear scar on steel ball were obtained using Phenom ProX desktop SEM operates (Nanoscience Instruments, Phoenix, AZ, USA) at 15 kV.

## 3. Results and Discussion

### 3.1. Materials Characterization

Figure 2a shows the spectrum for the synthesised alkyne functionalities, DiPPOH. Few peaks can be observed that can prove the success of DiPPOH synthesised. The synthesised DiPPOH is very crucial in order to provide the alkyne functionalities to the graphene oxide (GO). The absorption peaks at 3282  $\text{cm}^{-1}$ , 2117 and 646  $\text{cm}^{-1}$  corresponding to the presence of  $\text{C}\equiv\text{C}$  terminal stretching,  $\text{C}\equiv\text{C}$

stretching and  $C\equiv C$  bending respectively [30]. Absorption peaks indicating the C–H stretching of alkanes can be seen at  $2958$  and  $2888\text{ cm}^{-1}$ . At around  $1024$  to  $1295\text{ cm}^{-1}$ , numbers of absorption peaks were observed, indicating the presence of C–O stretching of alcohol. The functional groups observed in spectrum of DiPPOH proved that the synthesis of DiPPOH was a success.



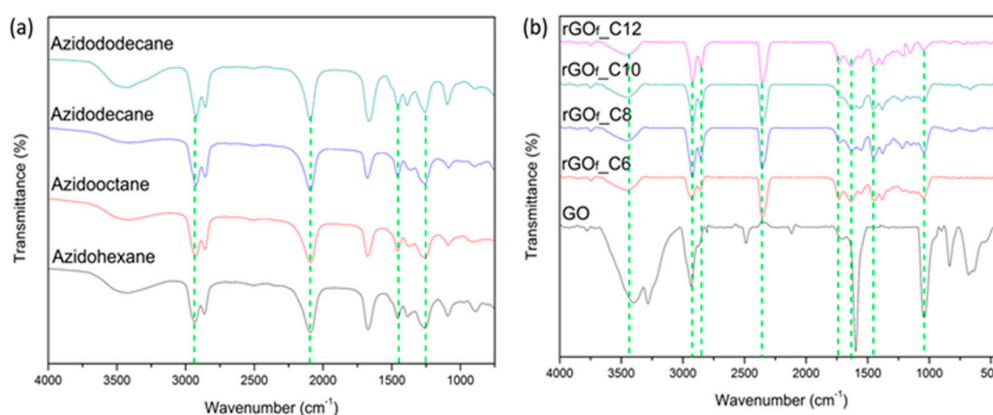
**Figure 2.** The FTIR spectra of (a) synthesized DiPPOH and (b) GO and  $GO_f$ .

Figure 2b shows the comparison of GO and  $GO_f$  spectrum. Few new peaks in  $GO_f$  spectrum can be observed that can prove the success of alkyne-functionalized GO when compared with GO. The absorption peaks at  $3282$ ,  $2112$  and  $676\text{ cm}^{-1}$  corresponding to the presence of  $C\equiv C$  terminal stretching,  $C\equiv C$  stretching and  $C\equiv C$  bending respectively. The intensity of C–H stretching at  $2930\text{ cm}^{-1}$  increased in  $GO_f$ , thus proving that the GO have been attached by the organic moiety synthesized, DiPPOH [27].

The intensities of the vibration peak of O–H groups at  $3418\text{ cm}^{-1}$  reducing proved that the O–H groups had been replaced by other functionalities. This may be due to the covalent functionalization that covalently attached the alkyne-functionalized molecule at the –OH groups on the surface of GO thus reducing their –OH group’s intensity. Lastly, the intensities of C–O stretching for ester was increased at  $1041\text{ cm}^{-1}$  proving that, the covalent attachment of the alkyne functionalities was a success.

Four main functionalities group can be observed in all four FTIR spectra of azide-functionalized alkyl; (a) azidohexane; (b) azidooctane; (c) azidododecane; (d) azidododecane, shown in Figure 3a. In all four different azide-functionalized alkyls, similar peaks can be observed. The peak at  $2900\text{ cm}^{-1}$  indicated the alkane stretching. The peak at  $2100\text{ cm}^{-1}$  are the major peaks that indicated the success of the azidation reaction, which is related to the azide stretching. The presence of azide group is very crucial in order to make sure that the cycloaddition reaction in click coupling between azide and alkyne can take place. Peaks at  $1455$  and  $1257\text{ cm}^{-1}$  represents the presence of methyl group alkane bending and aliphatic amine stretching respectively [26].

Figure 3b showed the FTIR spectrum of GO and four different  $rGO_f$ . All the four final products,  $rGO_f$ ;  $rGO_{f\_C6}$ ,  $rGO_{f\_C8}$ ,  $rGO_{f\_C10}$ , and  $rGO_{f\_C12}$  have almost similar peaks. Four main oxygen-containing functionalities group of GO can be observed in the FTIR spectrum presented in Figure 3b. The peaks at  $1725$  and  $1624\text{ cm}^{-1}$  were indicated to the stretching of C=O and the stretching of aromatic C=C respectively. The presence of peaks at  $1051$  and  $3418\text{ cm}^{-1}$  related to the stretching of C–O groups and O–H groups respectively.



**Figure 3.** The FTIR spectra of synthesized (a) azide-functionalized alkyl and (b) GO and rGO<sub>f</sub>.

For all four different rGO<sub>f</sub>, one crucial peak can be seen at  $2358\text{ cm}^{-1}$  indicating the stretching of C–N, proving the success of azide-alkyne coupling reaction on the GO sheets [27,31]. The intensities of the peaks indicating the presence of oxygen-containing functionalities showed a dramatic reduction from GO to rGO<sub>f</sub>. The intensities of the peak indicated to O–H of carboxylic acid groups at  $3418\text{ cm}^{-1}$  was reduced in broadness due to esterification. This may be due to the covalent functionalization that covalently attached the alkyne-functionalized molecule at the –OH groups on the surface of GO, thus reducing their –OH group’s intensity. However, the peak at  $1725\text{ cm}^{-1}$  indicated the stretching of C=O remains the same from GO to rGO<sub>f</sub>. These observations proved that C=O stretch of esters remains throughout the functionalization process. The functionalization of GO introduces new absorption peaks, apparently arising from the azidoalkyl into the products. For example, the doublet at  $2918$  and  $2850\text{ cm}^{-1}$  is indicated to the stretching of asymmetric C–H of alkanes in azidoalkyl. Absorption peak on all four different rGO<sub>f</sub> at  $1451\text{ cm}^{-1}$  related to the presence of C–H bend of alkane, proving that it has been successfully attached on GO.

The changes in the structure of the samples can be further studied by performing the XRD measurement. The XRD patterns for GO and rGO<sub>f</sub> is shown in Figure 4a. For GO, a broad peak at  $2\theta = 10.0^\circ$  can be observed, referring to a d-spacing of  $0.860\text{ nm}$ . The peak of GO was not observed in all the four different final products, rGO<sub>f</sub>. rGO<sub>f</sub> shows a new diffraction peak at  $2\theta = 19.9^\circ$ , referring to a d-spacing of  $0.818\text{ nm}$ . Reduction in the d-spacing after functionalization, indicated that upon functionalization, the structure of the samples was changed due to the amorphization of the material by introducing the organic moiety into the interlayer spacing of GO.

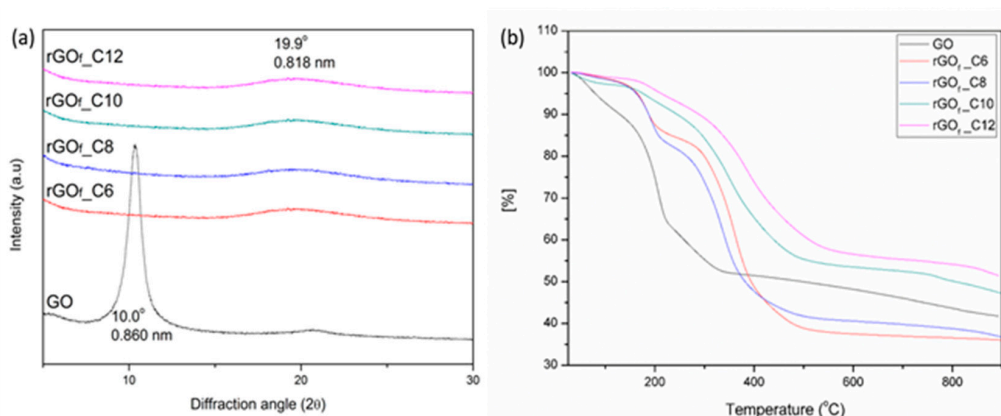


**Figure 4.** The (a) XRD patterns of GO and rGO<sub>f</sub> and (b) Thermal gravimetric analysis (TGA) diagram of GO and rGO<sub>f</sub>.

TGA diagram of GO and four different  $rGO_f$  are shown in Figure 4b. Firstly, the loss occurred at the temperature below 125 °C, primarily due to the loss of water molecules. Mass loss below 125 °C indicated that the content of adsorbed water for  $rGO_f$  was lower when compared to GO. It shows that  $rGO_f$  has lower water content than GO. This can prove that the hydroxyl groups in the  $rGO_f$  have been reduced by covalent functionalization of the organic moiety on the surface of GO [27,32]. Secondly, the unstable oxygen-containing functional groups will be thermally decomposed at a temperature of 225 °C [32,33]. Weight loss of  $rGO_f$  at 225 °C was very low compared to weight loss of GO. It proved that upon functionalization of GO, the oxygen-containing functional groups were also reduced during the click-coupling reaction.

To study the morphology of the  $rGO_f$ , FESEM was carried out, and the images are shown in Figure 5. All the four different  $rGO_f$  have almost similar SEM images. Fluffy aggregates on  $rGO_f$  can be clearly observed due to the presence of organic moiety on their surfaces [27]. The FESEM image of  $rGO_f$  shows that functionalization was successfully done by decorating organic molecules on the GO.

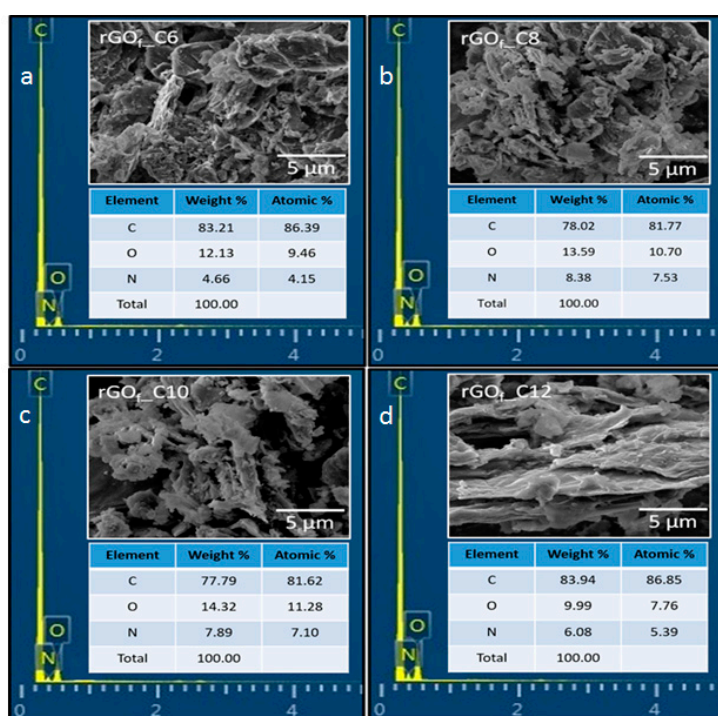


**Figure 5.** The FESEM images including EDX spectra of four different  $rGO_f$  with magnification of 50,000 $\times$ , (a)  $rGO_f$ \_C6, (b)  $rGO_f$ \_C8, (c)  $rGO_f$ \_C10 and (d)  $rGO_f$ \_C12.

The EDX analysis proved the appearance of element nitrogen, N in the  $rGO_f$ . It proved that the  $rGO_f$  has been decorated with a triazole ring that results from the reaction between alkyne and azide functionalities. Previous results of FTIR that has been discussed earlier proved that the N detected were groups of azide. Besides that, there is no trace of the Cu element in the  $rGO_f$ , proving that there are no residues of Cu that was used as the catalyst in the click coupling reaction left.

### 3.2. Dispersibility Test

Simplest qualitative test was carried out to determine whether the reduced functionalized GO,  $rGO_f$  has better dispersibility in oil than GO. The dispersibility of GO and four different  $rGO_f$  in oil was observed. Upon preparation of the dispersibility test, GO and all four different  $rGO_f$  separately dispersed in base oil subjected to the same sonication time. After sonication, it can be seen that GO cannot be uniformly dispersed in base oil, but for the  $rGO_f$ , it can easily disperse in the base oil. After one month of observation, it can be observed that the GO in base oil sedimented to the bottom

and while the  $rGO_f$  is still uniformly dispersed in base oil. Comparisons between GO and the four different  $rGO_f$  before and after 1 month are shown in Figure 6. It proved that upon functionalization, the dispersibility of the  $rGO_f$  in the base oil improved.

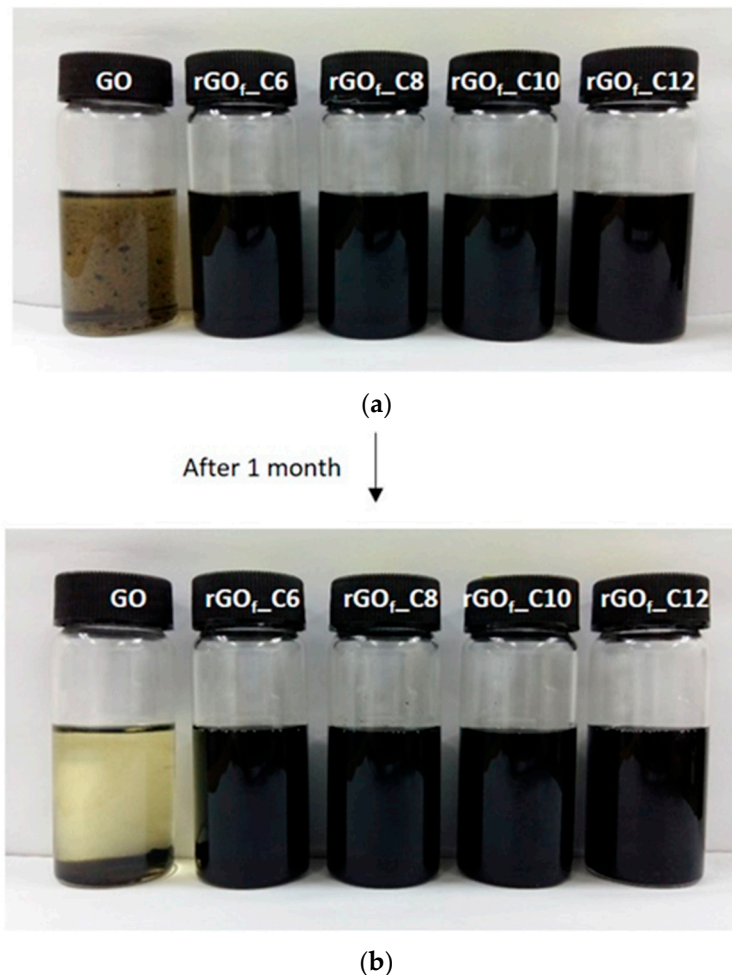


**Figure 6.** The GO and four different  $rGO_f$  dispersed in base oil (a); after 1 month (b).

### 3.3. Tribological Characterization

The coefficient of friction, CoF data were collected after a four-ball friction test. The variation of CoF with different  $rGO_f$  in the base oil was measured by applying 400 N load.

Figure 7 presents the CoF as a function of time for base oil, base oil with GO and also base oil with four different  $rGO_f$ . The experiments were repeated three times with fixed load to check the stability of the CoF value. From the results where the variation of mean and standard variation values was calculated, it can be noted that the lubricant yielded consistent CoF value over multiple runs with the maximum deviation of  $7.662 \times 10^{-3}$ . The results of CoF at concentration of 0.01 wt % are summarised in Table 1.

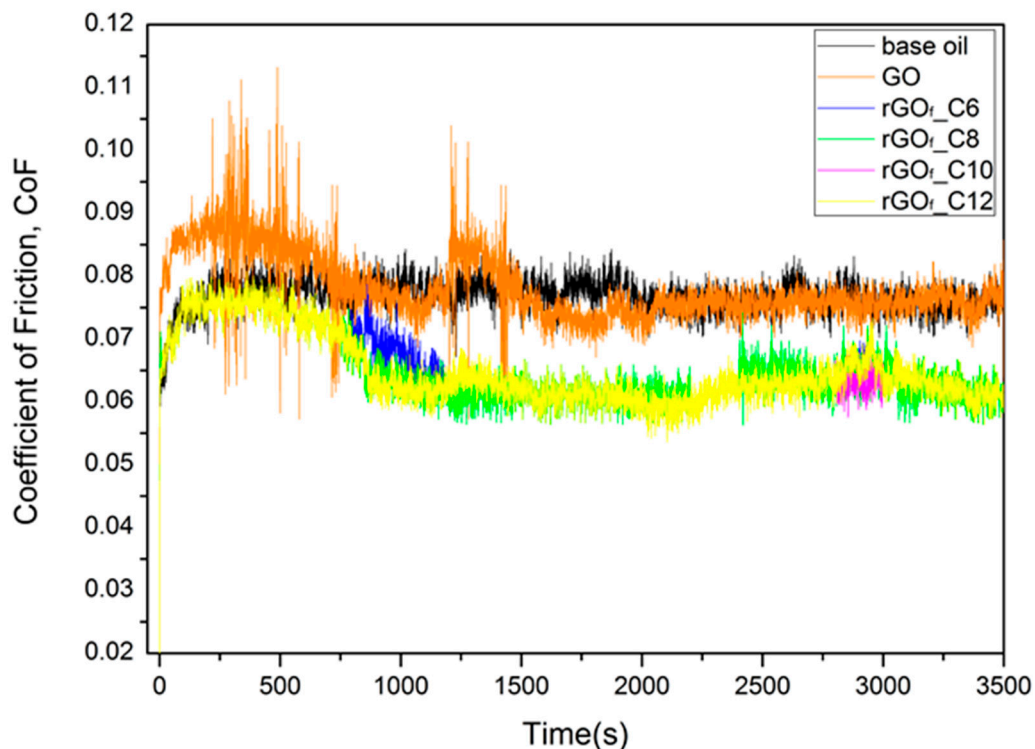


**Figure 7.** The coefficient of friction (CoF) of base oil with GO and four different  $rGO_f$ .

**Table 1.** Average Coefficient of Friction, CoF and difference in percentage for all the prepared samples.

Sample	Average Coefficient of Friction, CoF	Difference (%)
Base oil	0.077	Benchmark
Base oil with GO	0.078	+0.779
Base oil with $rGO_f$ _C6	0.065	−14.86
Base oil with $rGO_f$ _C8	0.065	−15.39
Base oil with $rGO_f$ _C10	0.065	−15.78
Base oil with $rGO_f$ _C12	0.065	−15.51

As shown in Table 1, the CoF of base oil was increased when added with GO. It can be due to the agglomeration of GO in the base oil that makes the oil not stable and all the GO sediment and do not provide lubrication [17]. Besides that, when the GO in the base oil agglomerate, it will result in rough contact surface that will results in increase of CoF. It is also clear that all these synthesised  $rGO_f$  causes a reduction in the CoF of the additive-added lubricant when compared to base oil without any  $rGO_f$ . It can be due to the tribochemical reaction that occurs between the organic moiety that has been attached on GO.

The polar groups on the  $rGO_f$  which results from the attachment of organic moiety on GO were assumed to tribochemically react with the positively charged metal surfaces reducing the friction through the formation of organic tribofilms [34].

In relation with average CoF obtained previously, the addition of  $rGO_f$  in base oil also has a direct impact on their wear scar diameter (WSD). From the SEM metallographs of wear surfaces on the steel balls used in four-ball test, the average wear scar diameter (WSD) were measured and the results were shown in Figure 8. The measurements were repeated three times to check the stability of the calculated WSD. From the results, it can be noted that the lubricant yielded consistent WSD value and the uncertainty level was below  $\pm 5\%$ . Wear scar diameter (WSD) of the steel ball was set as the benchmark to calculate the reduction in WSD after the addition of four different  $rGO_f$  at 0.01 wt %.

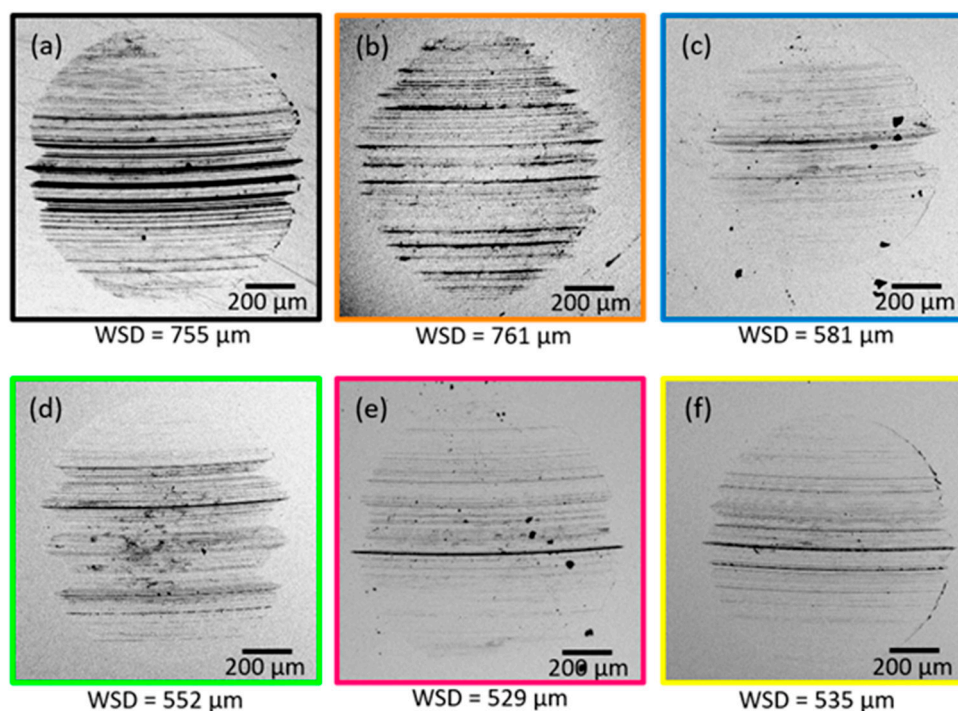


**Figure 8.** SEM metallographs of wear surfaces with GO and four different rGO<sub>f</sub> at 0.01 wt % in base oil (a) base oil; (b) GO; (c) rGO<sub>f</sub>-C6; (d) rGO<sub>f</sub>-C8; (e) rGO<sub>f</sub>-C10 and (f) rGO<sub>f</sub>-C12.

When compared to the WSD of base oil, all the four different rGO<sub>f</sub> were effectively reduced the WSD when they were added into the base oil. However, similar to the CoF value, the WSD for base oil that was added with GO also slightly increased. The smallest WSD can be observed with the used of rGO<sub>f</sub>-C10 that gave the highest reduction of WSD, which is about 30%. For rGO<sub>f</sub>-C6, rGO<sub>f</sub>-C8 and rGO<sub>f</sub>-C12, their reductions of WSD were 23%, 27% and 29% respectively. The trend in reduction of WSD for all the prepared samples were similar to the trend in reduction of CoF. Significant reduction of WSD for all the prepared samples can be observed when compared to the WSD of base oil without any addition of rGO<sub>f</sub> and also base oil that was added with GO.

#### 4. Conclusions

The functionalization of solid material by attachment of organic moiety was proved to effectively improve their tribological properties by formation of organic tribofilm. The tribology tests confirmed a good reduction in friction and wear can be accomplished with base oil formulated with functionalized graphene oxide. Their good friction properties also tribute to good anti-wear properties. Different rGO<sub>f</sub> with variations in their alkyl chain gives different values of CoF and WSD. The highest reduction in both CoF and WSD can be seen with the use of C10 attached on rGO<sub>f</sub>. The highest recorded reduction of CoF and WSD were 16% and 30% respectively. The outcomes apparently confirmed that graphene sheets attached with organic moiety in oil create protective films with ease to avoid the rubbing surfaces from coming into direct contact and, by that, completely enhances the tribology behaviour of the oil.

**Acknowledgments:** The authors are pleased to acknowledge the University of Malaya and Nanotechnology and Catalysis Research Centre (NANOCAT). This work was financially supported by the University of Malaya Grand Challenge Grant (Grant No. GC001A-14AET) and University of Malaya Postgraduate Research Grant (Grant No. PG058-2015B).

**Author Contributions:** Nurul Athirah Ismail and Samira Bagheri contributed equally to this manuscript.

**Conflicts of Interest:** The authors declare no conflict of interest.

## References

1. Holmberg, K.; Andersson, P.; Erdemir, A. Global energy consumption due to friction in passenger cars. *Tribol. Int.* **2012**, *47*, 221–234. [[CrossRef](#)]
2. Holmberg, K.; Erdemir, A. Global impact of friction on energy consumption, economy and environment. *FME Trans.* **2015**, *43*, 181–185.
3. Berman, D.; Erdemir, A.; Sumant, A.V. Graphene: A new emerging lubricant. *Mater. Today* **2014**, *17*, 31–42. [[CrossRef](#)]
4. Eswaraiah, V.; Sankaranarayanan, V.; Ramaprabhu, S. Graphene-based engine oil nanofluids for tribological applications. *ACS Appl. Mater. Interfaces* **2011**, *3*, 4221–4227. [[CrossRef](#)] [[PubMed](#)]
5. Fleischauer, P.; Hilton, M. Applications of space tribology in the USA. *Tribol. Int.* **1990**, *23*, 135–139. [[CrossRef](#)]
6. Peng, D.-X.; Chen, C.-H.; Kang, Y.; Chang, Y.-P.; Chang, S.-Y. Size effects of SiO<sub>2</sub> nanoparticles as oil additives on tribology of lubricant. *Ind. Lubr. Tribol.* **2010**, *62*, 111–120. [[CrossRef](#)]
7. Chen, S.; Liu, W.; Yu, L. Preparation of ddp-coated pbs nanoparticles and investigation of the antiwear ability of the prepared nanoparticles as additive in liquid paraffin. *Wear* **1998**, *218*, 153–158. [[CrossRef](#)]
8. Lu, H.F.; Fei, B.; Xin, J.H.; Wang, R.H.; Li, L.; Guan, W.C. Synthesis and lubricating performance of a carbon nanotube seeded miniemulsion. *Carbon* **2007**, *45*, 936–942. [[CrossRef](#)]
9. Holmberg, K.; Ronkainen, H.; Matthews, A. Tribology of thin coatings. *Ceram. Int.* **2000**, *26*, 787–795. [[CrossRef](#)]
10. Crawford, J.; Psaila, A.; Orszulik, S. Miscellaneous additives and vegetable oils. In *Chemistry and Technology of Lubricants*; Springer: Dordrecht, The Netherlands, 1997; pp. 181–202.
11. Jiang, W.; Nadeau, G.; Zaghbi, K.; Kinoshita, K. Thermal analysis of the oxidation of natural graphite—Effect of particle size. *Thermochim. Acta* **2000**, *351*, 85–93. [[CrossRef](#)]
12. Ren, P.-G.; Yan, D.-X.; Ji, X.; Chen, T.; Li, Z.-M. Temperature dependence of graphene oxide reduced by hydrazine hydrate. *Nanotechnology* **2010**, *22*, 055705. [[CrossRef](#)] [[PubMed](#)]
13. Lee, C.; Li, Q.; Kalb, W.; Liu, X.-Z.; Berger, H.; Carpick, R.W.; Hone, J. Frictional characteristics of atomically thin sheets. *Science* **2010**, *328*, 76–80. [[CrossRef](#)] [[PubMed](#)]
14. Senatore, A.; D’Agostino, V.; Petrone, V.; Ciambelli, P.; Sarno, M. Graphene oxide nanosheets as effective friction modifier for oil lubricant: Materials, methods, and tribological results. *ISRN Tribol.* **2013**, *2013*, 425809. [[CrossRef](#)]
15. Wintterlin, J.; Bocquet, M.-L. Graphene on metal surfaces. *Surf. Sci.* **2009**, *603*, 1841–1852. [[CrossRef](#)]
16. Ramanathan, T.; Abdala, A.; Stankovich, S.; Dikin, D.; Herrera-Alonso, M.; Piner, R.; Adamson, D.; Schniepp, H.; Chen, X.; Ruoff, R. Functionalized graphene sheets for polymer nanocomposites. *Nat. Nanotechnol.* **2008**, *3*, 327–331. [[CrossRef](#)] [[PubMed](#)]
17. Lin, J.; Wang, L.; Chen, G. Modification of graphene platelets and their tribological properties as a lubricant additive. *Tribol. Lett.* **2011**, *41*, 209–215. [[CrossRef](#)]
18. Bhushan, B.; Gupta, B.K. *Handbook of Tribology: Materials, Coatings, and Surface Treatments*; Krieger Publishing Company: Malabar, FL, USA, 1991.
19. Huang, H.; Tu, J.; Gan, L.; Li, C. An investigation on tribological properties of graphite nanosheets as oil additive. *Wear* **2006**, *261*, 140–144. [[CrossRef](#)]
20. Martorana, P.; Bayer, I.S.; Steele, A.; Loth, E. Effect of graphite and carbon nanofiber additives on the performance efficiency of a gear pump driven hydraulic circuit using ethanol. *Ind. Eng. Chem. Res.* **2010**, *49*, 11363–11368. [[CrossRef](#)]
21. Zhang, W.; Zhou, M.; Zhu, H.; Tian, Y.; Wang, K.; Wei, J.; Ji, F.; Li, X.; Li, Z.; Zhang, P. Tribological properties of oleic acid-modified graphene as lubricant oil additives. *J. Phys. D Appl. Phys.* **2011**, *44*, 205303. [[CrossRef](#)]
22. Ou, J.; Wang, J.; Liu, S.; Mu, B.; Ren, J.; Wang, H.; Yang, S. Tribology study of reduced graphene oxide sheets on silicon substrate synthesized via covalent assembly. *Langmuir* **2010**, *26*, 15830–15836. [[CrossRef](#)] [[PubMed](#)]
23. Gaylord, N.G. Reduction with complex metal hydrides. *J. Chem. Educ.* **1957**, *34*, 367. [[CrossRef](#)]
24. Truce, W.E.; Birum, G.; McBee, E. Chlorination of dimethyl sulfide and some of its derivatives with sulfuric chloride and thionyl chloride. *J. Am. Chem. Soc.* **1952**, *74*, 3594–3599. [[CrossRef](#)]
25. Freeman, J.; Smith, M. The preparation of anhydrous inorganic chlorides by dehydration with thionyl chloride. *J. Inorg. Nucl. Chem.* **1958**, *7*, 224–227. [[CrossRef](#)]

26. Liu, D.; Bielawski, C.W. Direct azidation of isotactic polypropylene and synthesis of 'grafted to' derivatives thereof using azide–alkyne cycloaddition chemistry. *Polym. Int.* **2016**. [[CrossRef](#)]
27. Namvari, M.; Namazi, H. Sweet graphene i: Toward hydrophilic graphene nanosheets via click grafting alkyne-saccharides onto azide-functionalized graphene oxide. *Carbohydr. Res.* **2014**, *396*, 1–8. [[CrossRef](#)] [[PubMed](#)]
28. Cao, Y.; Lai, Z.; Feng, J.; Wu, P. Graphene oxide sheets covalently functionalized with block copolymers via click chemistry as reinforcing fillers. *J. Mater. Chem.* **2011**, *21*, 9271–9278. [[CrossRef](#)]
29. Kou, L.; He, H.; Gao, C. Click chemistry approach to functionalize two-dimensional macromolecules of graphene oxide nanosheets. *Nano-Micro Lett.* **2010**, *2*, 177–183. [[CrossRef](#)]
30. Wang, H.-X.; Zhou, K.-G.; Xie, Y.-L.; Zeng, J.; Chai, N.-N.; Li, J.; Zhang, H.-L. Photoactive graphene sheets prepared by “click” chemistry. *Chem. Commun.* **2011**, *47*, 5747–5749. [[CrossRef](#)] [[PubMed](#)]
31. Dondoni, A. Triazole: The keystone in glycosylated molecular architectures constructed by a click reaction. *Chem.–Asian J.* **2007**, *2*, 700–708. [[CrossRef](#)] [[PubMed](#)]
32. Chen, J.; Yao, B.; Li, C.; Shi, G. An improved hummers method for eco-friendly synthesis of graphene oxide. *Carbon* **2013**, *64*, 225–229. [[CrossRef](#)]
33. Marcano, D.C.; Kosynkin, D.V.; Berlin, J.M.; Sinitskii, A.; Sun, Z.; Slesarev, A.; Alemany, L.B.; Lu, W.; Tour, J.M. Improved synthesis of graphene oxide. *ACS Nano* **2010**, *4*, 4806–4814. [[CrossRef](#)] [[PubMed](#)]
34. Simic, R.; Kalin, M. Comparison of alcohol and fatty acid adsorption on hydrogenated dlc coatings studied by afm and tribological tests. *Stroj. Vestnik-J. Mech. Eng.* **2013**, *59*, 707–718. [[CrossRef](#)]



© 2017 by the authors. Licensee MDPI, Basel, Switzerland. This article is an open access article distributed under the terms and conditions of the Creative Commons Attribution (CC BY) license (<http://creativecommons.org/licenses/by/4.0/>).